Resolving Singular Forces in Cavity Flow: Multiscale Modeling from Atomic to Millimeter Scales

Xiaobo Nie,[1] Mark O. Robbins,[1,2] and Shiyi Chen[2,3]
[1]Department of Physics and Astronomy, The Johns Hopkins University, Baltimore, Maryland 21218, USA
[2]Department of Mechanical Engineering, The Johns Hopkins University, Baltimore, Maryland 21218, USA
[3]CoE and CCSE, Peking University, Beijing, China
(Received 8 August 2005; published 3 April 2006)

Flow driven by moving a wall that bounds a fluid-filled cavity is a classic example of a multiscale problem. Continuum equations predict that every scale contributes roughly equally to the total force on the moving wall, leading to a logarithmic divergence, and that there is an infinite hierarchy of vortices at the stationary corners. A multiscale approach is developed that retains an atomistic description in key regions. Following the stress over more than six decades in length in systems with characteristic scales of up to millimeters and milliseconds allows us to resolve the singularities and determine the force for the first time. We find a universal dependence on the macroscopic Reynolds number, and large atomistic effects that depend on wall velocity and interactions.

DOI: 10.1103/PhysRevLett.96.134501 PACS numbers: 47.11.St, 47.61.Cb, 68.08.−p, 83.50.Rp

Processes that span a wide range of length scales pose profound theoretical challenges [1,2]. The different length scales must be followed with different time resolutions and may require qualitatively different descriptions of matter. For example, discrete atomistic effects may be important in regions of high stress or rapid spatial variation, while other regions are most naturally and efficiently modeled as a continuous medium. Important examples of such problems include adhesion and friction [3,4], deformation of crystalline solids [5,6], distribution and flow of charges at biological interfaces, flow near solid surfaces [7], and the many cases where continuum equations lead to singularities.

Several innovative paradigms for bridging between atomistic and macroscopic scales have been proposed in recent years, and tested against purely atomistic simulations in small idealized systems [8–15]. A few have been applied to specific problems with a large range of scales. Notable examples include calculations of crack propagation in silicon that include electronic structure near the crack tip [16], and calculations of indentation with the quasicontinuum method [17]. However, these applications have only reached micrometer length and nanosecond time scales, and the main effect of large scales is to provide appropriate boundary conditions for the atomistic region.

In this Letter we consider a classic problem in fluid mechanics where all length scales contribute equally: the force on a moving boundary of a fluid-filled cavity. Using different spatial and temporal resolutions in different regions allows us to treat cavities with dimensions on the order of millimeters and characteristic times of tens of milliseconds. Our multiscale approach accelerates the calculation by more than 14 orders of magnitude compared to brute force atomistic simulations. Spanning many decades in length scale allows us to build a simple scaling relation for the total force F that captures both atomistic effects and the influence of the only parameter in continuum theory, Reynolds number.

Cavity flow has intrigued scientists because of singularities that cannot be resolved by purely continuum methods. Figure 1(a) illustrates the cavity geometry. The top wall is displaced to the right at fixed velocity **U** and the other walls

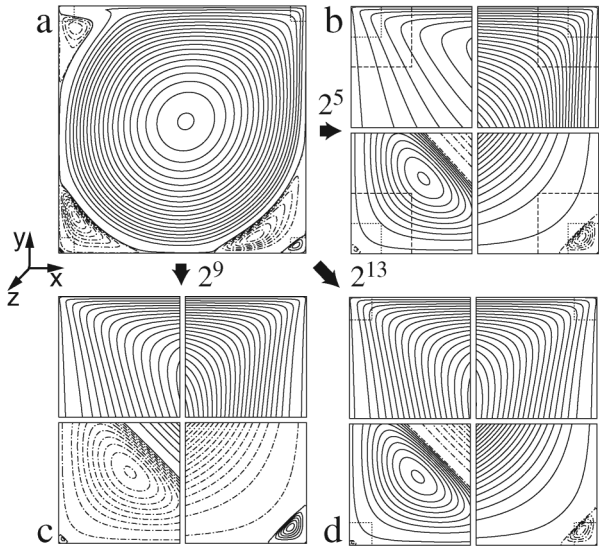

FIG. 1. Geometry and streamlines for cavity flow at $\mathrm{Re} \equiv \rho UL/\mu = 6400$. (a) The square cavity has edge $L = 10^6\sigma \sim 0.3$ mm in the x-y plane, the top wall moves to the right at speed U, the flow is independent of z, and the natural time scale to reach steady state flow is ~40 ms. Solid (dash-dotted) streamlines indicate clockwise (counter-clockwise) flow. In (b), (c), (d), flow near each corner is magnified by the indicated factor. The coupling of different resolutions is illustrated in (b). The coarser solution provides boundary conditions along the outer boundary of the finer grid (dashed lines) and obtains them along the dotted lines. In (d), dotted lines indicate the boundaries of the $\sim 12\sigma$ wide regions that are treated atomistically.

are stationary. The traditional continuum approach to this problem uses the Navier-Stokes (NS) equations and no-slip boundary conditions at the walls [18–21]. The no-slip condition requires that the fluid velocity $\mathbf{u}$ vanishes near static walls, and equals $\mathbf{U}$ at the moving wall. The discontinuity in boundary condition at corners between moving and fixed walls causes the stress to diverge as the inverse of the distance from the corner, r. The total force on the wall is the integral of the stress. Since each factor of 2 in r gives the same contribution to F, it diverges logarithmically in continuum theory.

Koplik and Banavar pioneered the use of molecular dynamics (MD) to study the stress singularities in cavity flow at atomistic scales [22]. They observed a breakdown of the no-slip boundary condition within atomic distances from the corner, and a corresponding saturation of the stress. Similar effects cut off stress singularities in the closely related problem of spreading fluids [23,24]. The purely atomistic approach used by Koplik and Banavar limited the cavity length to $L = 17\sigma$, where $\sigma \sim 0.3$ nm corresponds to a molecular diameter. We recently extended L to $250\sigma \sim 75$ nm using a hybrid method that treated singular regions atomistically and the remainder of the cavity as a continuum. This approach allowed us to analyze the breakdown of the continuum boundary conditions over a wider range of U, and to determine its microscopic origins [25]. The stress deviates from the singular continuum solution for $r < S(U)$. At low U, the intrinsic discreteness of atomic fluids leads to $S \sim \sigma$. At large U, the interfacial stress is high enough to produce non-Newtonian effects [7], and S rises linearly with U.

Despite the success of this previous work, there has been no study of the total force on the moving wall. This is because determining F over a significant range of U and Re requires study of cavities with dimensions up to the millimeter scale. To make this possible, two major improvements must be made on previous work. The first is to vary the resolution in the continuum region to efficiently describe the rapid increase in velocity gradients near the singular corners. We chose to do this using a local refinement approach [26]. The second is to span the wide range of time scales associated with different spatial resolutions. While the motion of atoms near the corner must be followed with time steps of order 10^{-14} s, the time for flows to equilibrate on millimeter scales, $\sim 100L/U$, may be on the order of seconds. To overcome this obstacle we use the optimum time step to obtain the steady state flow at each spatial scale, and then enforce self-consistency between scales.

The details of our approach and a sample flow field are illustrated in Fig. 1. At the continuum scale the flow is independent of z, and satisfies the NS equations with vicosity μ, fixed density ρ, and no-slip boundary conditions. At each scale the NS equations are discretized on a square grid of cells with width h, and the steady state flow is obtained using an artificial compressibility method [27] with time step of $\frac{1}{4}$–$\frac{1}{2}$ h/U. On the coarsest scale $h = L/256$. This resolution is inadequate near the corners, where h is decreased by successive factors of two using an iterative refinement scheme.

At each stage of the iteration, solutions at two resolutions provide boundary conditions for each other. The geometry is illustrated in Fig. 1(b). Both resolutions use a 64 by 64 array of square cells. The finer grid lies in the inner quarter of the coarse grid (dashed lines), and receives boundary conditions on its outer edge. It in turn provides boundary conditions for the coarser grid along the dotted lines. The overlap region between dashed and dotted lines prevents discontinuities due to sudden changes in resolution [9,10,12].

This refinement scheme is iterated until the overlap region reaches nanometer scales. There the finest resolution results are obtained from MD simulations that can be extended all the way into the corner [Fig. 1(d)]. At the outer edge of the MD region the mean atomic velocity is constrained to follow the finest continuum solution ($h = 0.95\sigma$) and particles are added or removed to match the continuum flux [9,25]. Average MD velocities provide boundary conditions for the continuum solution along an inner square whose edge is 6 cells long. A global steady state solution is obtained by iterating from coarsest to finest scale and then back until all boundary conditions are consistent. This typically requires 10 to 20 iterations, depending on the desired accuracy.

To obtain a smooth solution, the continuum model must accurately describe the atomistic behavior at the outer boundary of the MD region. This requires consistent choices of μ and molecular interactions. Following previous work [22,25], we consider fluid atoms of mass m interacting with a Lennard-Jones (LJ) potential of characteristic energy ϵ and diameter σ. The potential is truncated at $r_c = 2.2\sigma$, and the mass density $\rho = 0.81 m\sigma^{-3}$. The geometry and interactions of the crystalline walls are chosen to produce a no-slip boundary condition far from the corner [25]. Discrete wall atoms are on the sites of a (111) surface of an fcc crystal of lattice constant 1.204σ and interact with the fluid with a LJ potential with energy $\epsilon_{\mathrm{wf}} = 0.95\epsilon$.

Within the MD region, the motion of particles is fully three-dimensional. However, the mean velocities are independent of z, and periodic boundary conditions with period L_z are applied in this direction. The equations of motion are integrated using the Verlet scheme with time step $0.005 t_{\mathrm{LJ}}$, where $t_{\mathrm{LJ}} \equiv (m\sigma^2/\epsilon)^{1/2}$ is the characteristic time of the LJ potential. One can show that the Stokes solution predicts a temperature rise that is independent of r and L, and proportional to the Brinkman number $\mathrm{Br} \equiv \mu U^2/T\kappa$, where $\kappa = 7.7 k_B/\sigma t_{\mathrm{LJ}}$ is the thermal conductivity and k_B is Boltzmann's constant. Atomistic simulations [22,25] show that the temperature rise is less than 10% for the largest velocities considered here, and that much larger rises have negligible effect on the stress and velocity fields [22]. We thus maintain a constant tempera-

ture $k_B T = 1.1\epsilon$ in the MD region using a Langevin thermostat [28] with damping rate $\Gamma = 1 t_{\mathrm{LJ}}^{-1}$. To avoid biasing the flow, the thermostat is only applied in the z direction. The dynamic viscosity [10] of the LJ fluid $\mu = 2.14\epsilon t_{\mathrm{LJ}} \sigma^{-3}$ is used in the NS equations. In general the atomistic region dominates the calculation time (70– >99%). The continuum calculation becomes more costly at high Reynolds number, while the atomistic calculation time grows with decreasing U because the averaging time or L_z must be increased in order to reduce statistical fluctuations.

Two lengths characterize transitions in flow behavior near each corner (Fig. 1). Inertial effects are significant for $r > r_I \equiv \mu/\rho U$, while deviations from continuum behavior occur for $r < S(U)$. At intermediate scales our results follow the analytic solution for Stokes (noninertial) flow [18]. Near the top corners the streamlines are scale invariant because $\mathbf{u}$ only depends on the angle relative to the moving wall. The stress diverges as $1/r$ since $\mathbf{u}$ changes by U over a length of order r. One efficient approach for obtaining accurate velocity fields in the center of the cavity is to subtract the Stokes singularity and compute the nonsingular remainder on a relatively coarse grid [21]. However, this approach does not remove the divergent contribution to F from small r.

A series of counter-rotating vortices forms in the Stokes regime near the bottom corners. The change in scale between panels in Fig. 1 was chosen to illustrate the predicted self-similarity under $r \rightarrow r/16.4$ and a change in direction of rotation [19,29]. To our knowledge, this hierarchy of vortices has not been observed in previous numerical studies of cavity flow. The vortices are cut off at $S(0) \sim \sigma$ by atomistic effects, and this is responsible for the small deviation between Figs. 1(c) and 1(d).

Figure 2(a) shows a plot of the shear stress τ along the moving wall at Reynolds number $\mathrm{Re} \equiv \rho U L/\mu = 6400$ as a function of distance r from the upper-left corner. Alternating colors are used for data from different resolutions to illustrate the smooth matching. The asterisks are from the force per unit area on wall atoms in the atomistic region. At intermediate scales, the stress follows the divergence predicted by the Stokes solution $\tau = 4\pi(\pi^2 - 4)^{-1} \mu U/r$ (straight line). At large scales the stress decays more slowly than $1/r$, and at $r < S \approx 2.2\sigma$ the stress singularity is cut off by atomistic effects. Figure 2(b) shows that changing Re by increasing L only changes the flow in the outer region. At scales of order $L/2$ the other corners become important, but for $r \ll L/2$ all results fall onto a common curve. This shows that S is independent of L and only depends on U and atomic properties.

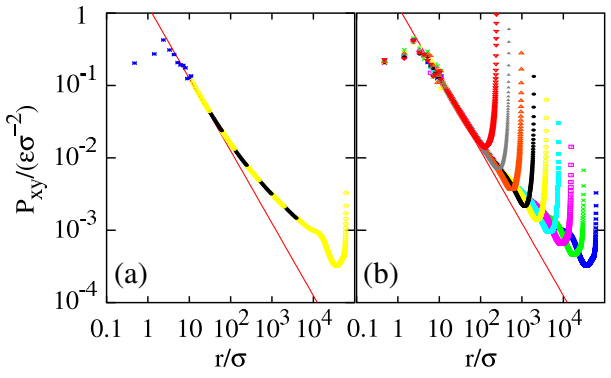

FIG. 2 (color online). Shear stress as a function of distance r from the upper-left corner for $U = 0.27\sigma/t_{\mathrm{LJ}}$. Qualitatively similar scaling occurs near the upper-right corner. In (a) $\mathrm{Re} = 6400$, $L = 6.25 \times 10^4 \sigma$, $r_I = 9.8\sigma$, $S \approx 2.2\sigma$, lines of alternating color indicate continuum results from successive resolutions, and asterisks show MD results. Results for $\mathrm{Re} = 25$ to 6400 obtained by increasing L by factors of two are compared in (b).

The total shear force on the moving wall is an integral of the shear stress along it. Figure 3 shows the force per unit length along the z direction, F, as a function of Re. If the Stokes solution applied, each factor of 2 in length scale would contribute the same force and the total would diverge. This divergence is cut off by atomistic effects at $r < S$ but inertial effects enhance the force from $r > r_I$. To determine F, one must resolve the inertial effects between r_I and $L = \mathrm{Re}\, r_I$ as well as the atomistic behavior at the corner. Our approach enables us to span this wide range of scales ($>10^5$) for the first time.

If atomistic effects were not important, the dimensionless force on the wall $f \equiv F/\mu U$ would only depend on Re. However, Fig. 3 shows that changing U at fixed Re produces large shifts in f. A complete description of f can be obtained by considering the separate contributions, f_i, of the three scaling regimes in the stress shown in Fig. 2. They are well separated as long as $\mathrm{Re} = L/r_I \gg 1$ and the Reynolds number at molecular scales $\mathrm{Re}_m \equiv S/r_I \ll 1$.

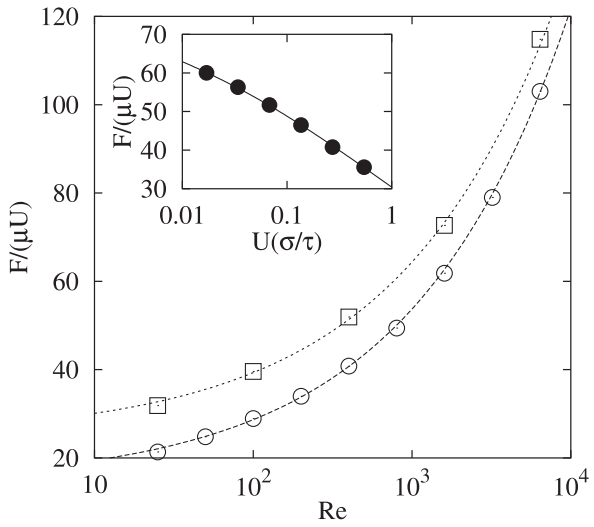

FIG. 3. Dimensionless force per unit length on the sliding wall $F/\mu U$ as a function of Reynolds number $\mathrm{Re} = \mu U L/\rho$. Results for $U = 0.27\sigma/t_{\mathrm{LJ}}$ (circles) and $U = 0.068\sigma/t_{\mathrm{LJ}}$ (squares) follow Eq. (1) (dashed lines) with $S = 2.2$ and 0.55, respectively. The inset compares the calculated force vs velocity at $\mathrm{Re} = 400$ (circles) to Eq. (1) (line).

The dependence on Re comes entirely from the outer region $r > r_I$, which is why curves for different U in Fig. 3 are related by a constant shift. As shown in Fig. 2(b), increasing Re extends the range of the inertial tail that contributes to the dimensionless force, causing $f_3(\mathrm{Re})$ to rise with Re. For $\mathrm{Re} > 10$ our numerical results are well described by $f_3 = a + b\mathrm{Re}^{\alpha}$ with $a = 3.85$, $b = 1.98$, and $\alpha = 0.434$.

In the inner region near each corner, $r < S$, the stress is determined entirely by U and atomic properties, such as t_{LJ}, σ, ρ, and wall geometry [Fig. 2(b)]. For fixed interactions, we can write the contribution from this regime as $f_1(Ut_{\mathrm{LJ}}/\sigma)$. In fact, we find f_1 has a constant value of about 4.3. The reason is that the range of integration grows linearly with S while the stress scales inversely with S. Indeed, assuming the stress for $r < S$ is equal to the Stokes stress at S yields $f_1 = 8\pi/(\pi^2 - 4) \approx 4.28$, which is consistent with the numerical results. The value of f_1 is as much as 20% of the total wall force in Fig. 3, yet it comes from an inner region that is never larger than a few molecular diameters. This is clear evidence of the direct effect of atomic scales on the macroscopic force.

In the intermediate region, $S < r < r_I$, the Stokes solution applies, and can be integrated to give $f_2(r_I/S) = 8\pi(\pi^2 - 4)^{-1}\ln(r_I/S)$. This term is responsible for the velocity dependence in the total dimensionless force:

$$\frac{F}{\mu U} = f_1 + \frac{8\pi}{\pi^2 - 4}\ln(r_I/S) + a + b\mathrm{Re}^{\alpha}. \qquad (1)$$

The ratio S/r_I reflects the range at which atomistic effects cut off the Stokes region, and decreases as U decreases. The inset to Fig. 3 shows that numerical results for the velocity dependence of F are consistent with $S = S_0 + kUt_{\mathrm{LJ}}$ with $S_0 = 0.3\sigma$ and $k = 7$. This form for S is consistent with our previous studies [25], which showed S approached a constant of atomic scale at low velocities and rose linearly with U at high velocities due to non-Newtonian effects.

Our multiscale method has allowed us to span the wide range of length scales ($>10^5$) that contribute to the drag force on the moving wall of an ideal cavity, and to extract a simple and accurate physical description [Eq. (1)] of the important contributions from each scale. We have used it to treat cavities with dimensions on the order of millimeters and natural time scales approaching seconds, and the approach is readily extended to still larger scales. Its major limitation is that it assumes a steady state solution, while cavity flow becomes unsteady at $\mathrm{Re} \gtrsim 8000$ [30]. It may be possible to extend simulations into the turbulent regime using ideas like the ''equation-free'' approach of Kevrekidis *et al.* [15]. Turbulent fluctuations occur on the longer time scales associated with coarser resolutions, and the finer scales can be iterated to a quasistatic state that follows the coarse solution. This would allow calculations with the same coarse time step that is used in a completely continuum description, while retaining the crucial atomic detail. We hope that our work encourages such efforts, as well as applications to other important multiscale problems such as contact-line motion and contact mechanics.

This material is based upon work supported by the U.S. National Science Foundation under Grants No. CMS-0103408, No. CTS-0320907, and No. PHY-99-07949.

[1] J. Glimm and D. H. Sharp, SIAM News **30**, No. 8, 4 (1997).
[2] T. Y. Hou, Int. J. Numer. Methods Fluids **47**, 707 (2005).
[3] M. Urbakh, J. Klafter, D. Gourdon, and J. Israelachvili, Nature (London) **430**, 525 (2004).
[4] B. Luan and M. O. Robbins, Nature (London) **435**, 929 (2005).
[5] M. D. Uchic, D. M. Dimiduk, J. N. Florando, and W. D. Nix, Science **305**, 986 (2004).
[6] J. Weiss and D. Marsan, Science **299**, 89 (2003).
[7] P. A. Thompson and S. M. Troian, Nature (London) **389**, 360 (1997).
[8] J. Li, D. Liao, and S. Yip, Phys. Rev. E **57**, 7259 (1998).
[9] X. B. Nie, S. Y. Chen, W. N. E, and M. O. Robbins, J. Fluid Mech. **500**, 55 (2004).
[10] S. T. O'Connell and P. A. Thompson, Phys. Rev. E **52**, R5792 (1995).
[11] N. G. Hadjiconstantinou and A. T. Patera, Int. J. Mod. Phys. C **8**, 967 (1997).
[12] E. G. Flekkoy, G. Wagner, and J. Feder, Europhys. Lett. **52**, 271 (2000).
[13] V. B. Shenoy, R. Miller, E. B. Tadmor, R. Phillips, and M. Ortiz, Phys. Rev. Lett. **80**, 742 (1998).
[14] W. Q. Ren and W. N. E, J. Comput. Phys. **204**, 1 (2005).
[15] I. G. Kevrekidis, C. W. Gear, and G. Hummer, AIChE J. **50**, 1346 (2004).
[16] J. Q. Broughton, F. F. Abraham, N. Bernstein, and E. Kaxiras, Phys. Rev. B **60**, 2391 (1999).
[17] J. Knap and M. Ortiz, Phys. Rev. Lett. **90**, 226102 (2003).
[18] G. K. Batchelor, *An Introduction to Fluid Dynamics* (Cambridge University Press, Cambridge, 1967).
[19] F. Pan and A. Acrivos, J. Fluid Mech. **28**, 643 (1967).
[20] U. Ghia, K. N. Ghia, and C. Y. Shin, J. Comput. Phys. **48**, 387 (1982).
[21] O. Betella and R. Peyret, Comput. Fluids **27**, 421 (1998); Int. J. Numer. Methods Fluids **36**, 125 (2001).
[22] J. Koplik and J. R. Banavar, Phys. Fluids **7**, 3118 (1995).
[23] J. Koplik, J. R. Banavar, and J. F. Willemsen, Phys. Rev. Lett. **60**, 1282 (1988).
[24] P. A. Thompson and M. O. Robbins, Phys. Rev. Lett. **63**, 766 (1989).
[25] X. B. Nie, S. Y. Chen, and M. O. Robbins, Phys. Fluids **16**, 3579 (2004).
[26] S. F. McCormick, *Multilevel Adaptive Methods for Partial Differential Equations* (SIAM, Philadelphia, 1989).
[27] R. Peyret and T. D. Taylor, *Computational Methods for Fluid Flow* (Springer-Verlag, New York, 1983).
[28] G. S. Grest and K. Kremer, Phys. Rev. A **33**, 3628 (1986).
[29] H. K. Moffatt, J. Fluid Mech. **18**, 1 (1964).
[30] W. Cazemier, R. W. C. P. Verstappen, and A. E. P. Veldman, Phys. Fluids **10**, 1685 (1998).